

Dustin Phillips¹ and Kevin Knupp
 Department of Atmospheric Science
 University of Alabama Huntsville

1. INTRODUCTION

In the late 1970s the convective system that is referred to as the bow echo was identified by Fujita (1978). It was identified as a type of convective storm structure associated with intense damaging winds or downburst (Johns 1993). As more of these systems were studied, a better understanding was made on their kinematic structure and dynamical processes. Bow echoes can range in size from 15 km to 150 km, and can occur at anytime of year (Klimowski et al. 2000). Much of the damage reported in the United States from non-tornadic winds is a result of bow echo systems.

The “model” bow echo evolves from a single or large group of strong convective cells, to a bow-shaped line segment, and finally, to a comma-shaped echo in its declining phase (Fujita, 1978). The development of a bow echo can be related to a number of different synoptic variables and conditions. Strong bow echoes that produce widespread damage can occur in strong migrating low pressure systems as well as in rather benign synoptic patterns.

During the Bow Echo and MCV Experiment (BAMEX) the ground-based platforms – the Mobile Integrated Profiling System (MIPS) and two NCAR MGLASS units – were deployed in advance of evolving mesoscale convective systems to monitor the environmental and storm properties of bow echo systems.

On 24 June 2003 the MIPS was deployed at a site just south of Fort Dodge in northwest Iowa, about 86 km from the Des Moines (DMX) WSR-88D radar. The NCAR MGLASS1 was deployed 76km to the west, and MGLASS2 was 176 km to the north. Around 0650 UTC, the MIPS acquired an excellent data set on a surging bow echo near the time of maximum radial velocity (exceeding 30 m s^{-1}) measured from the DMX WSR-88D. The peak updraft within deep convection, $\sim 20 \text{ m s}^{-1}$, occurred about 10 minutes after the gust front arrival. The maximum surface wind gust of 24 m s^{-1} was measured about 10 minutes after the gust front arrival, well behind the leading edge within relatively heavy precipitation.

The goals of this paper are (1) to analyze MIPS data to define the environment preceding the bow echo (GLASS soundings and the radiometer (MPR)), and to describe the environment in the wake of the bow echo; and (2) to describe the internal storm structure from an analyses of MIPS 915 MHz profiler and electric field mill measurements, MPR

¹Corresponding authors address: Dustin Phillips, 320 Sparkman Dr. NSSTC, Huntsville, AL 35805; email phillips@nsstc.uah.edu

measurements, ceilometer measurements, supplemented with Doppler analyses from the DMX WSR-88D and the NCAR Eldora airborne Doppler radar.

2. STORM ENVIRONMENT

Figure 1 displays a skew-T plot from MGLASS1 at 0450 UTC. This sounding was launched about two hours before arrival over the MIPS and one hour before passing over the MGLASS1 location. A shallow mixed layer extends from the surface to 925 hPa. Above this, a moist adiabatic layer is capped by a stable layer centered near 800 hPa. The MCS anvil cloud base is apparent near 400 hPa, and precipitation evaporation is suggested from anvil base to about 470 hPa. Although this is not a full tropospheric sounding, we estimate the CAPE value to be about 3000 J kg^{-1} . The lifted index for a surface-based parcel is appreciable at about $-10 \text{ }^\circ\text{C}$. Veering and speed shear is most significant below 850 hPa. Middle tropospheric flow is uniform southwesterly near $25\text{-}30 \text{ m s}^{-1}$, and overlies a low level jet of 25 m s^{-1} , centered near 1 km AGL.

A time vs. height section of horizontal flow from the 915 MHz profiler (Fig. 3) reveals three prominent features: 1) A low level jet (25 m s^{-1}) exists near 1 km

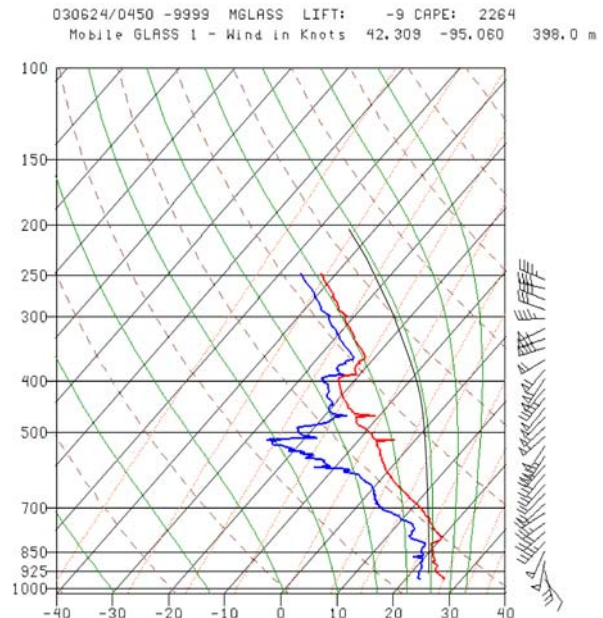


Figure 1: MGLASS1 Sounding from 0450 UTC. The surface based parcel has been added (black). The anvil level is located at approximately 400 mb.

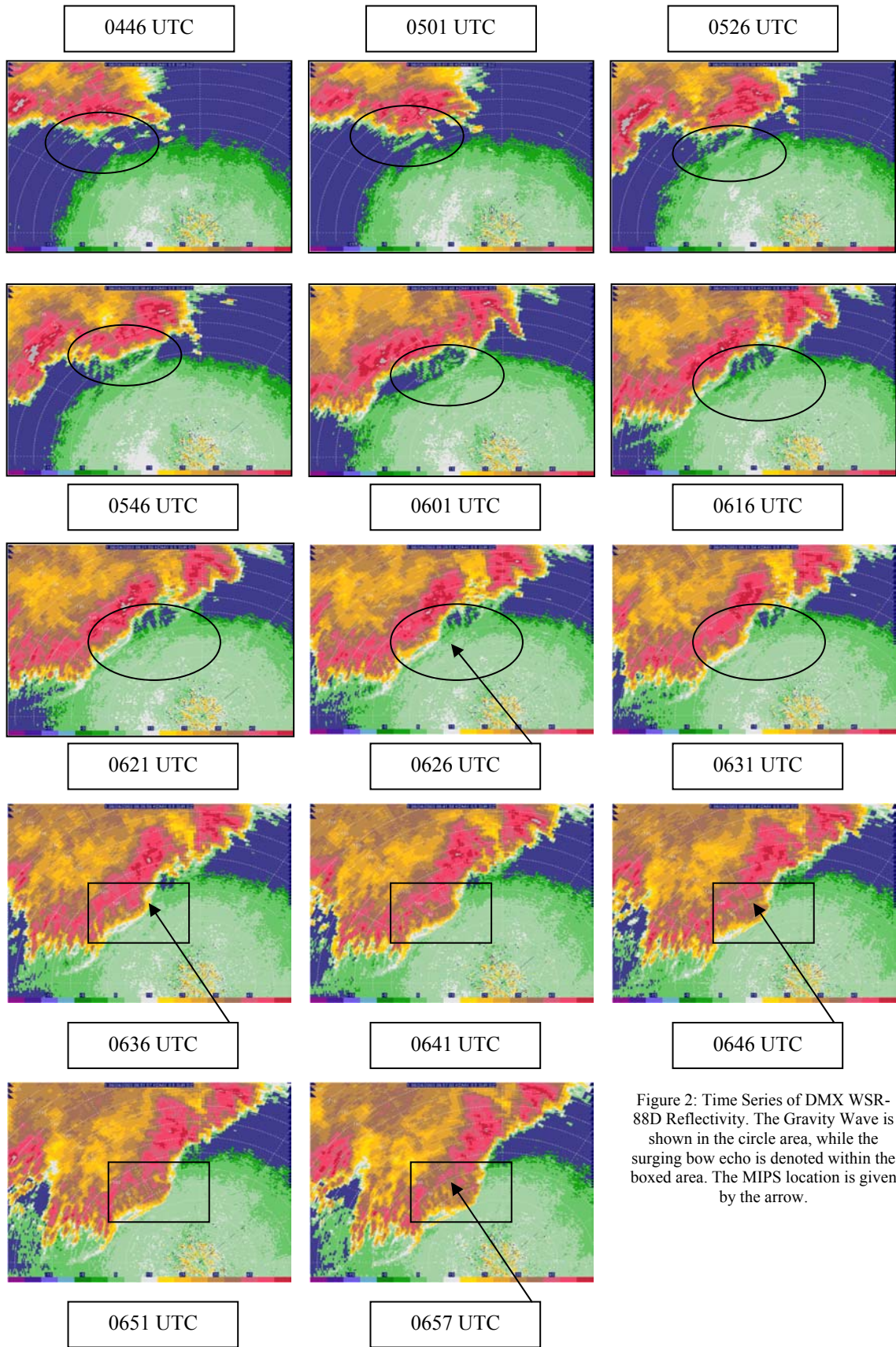


Figure 2: Time Series of DMX WSR-88D Reflectivity. The Gravity Wave is shown in the circle area, while the surging bow echo is denoted within the boxed area. The MIPS location is given by the arrow.

AGL. 2) Strong southwesterly midlevel flow of 25 m s⁻¹ was sampled at the back of the system, but this jet did

not descend to low levels. 3) The most significant wind change was confined to the lowest 2 km, where strong southerly winds (and the southerly jet near 1 km AGL) were replaced by weaker northerly flow.

The inversion layer shown in the MGLASS1 sounding is also visible as enhanced return power (SNR) from the 915 MHz profiler, shown in time-height section format in Fig. 4. At 0520 UTC, layers of enhanced SNR are located near 1.5, 2.0 and 3.5 km. Enhanced SNR over the lowest 1 km was produced by Rayleigh scatter from insects. The layer at 2 km corresponds to the inversion near 800 hPa (MGLASS1 sounding) and was produced by Bragg scatter. This layer moved upward to 2.5-3.0 km by 0540, suggesting that the environment changed rapidly in advance of the bow echo. By 0615 UTC, a deeper layer of enhanced SNR (indicative of shallow convective structures) had developed within the 2.5-4.0 km layer, suggesting lifting and associated destabilization immediately in advance of the bow echo. This destabilization shown by the SNR can be correlated to an increase in the vertically integrated vapor (VINT), and vertical integrated liquid (LINT) measured by the MPR for the same time period (figure 7). For this time period the VINT increased by approximately 0.6 cm, as well as the LINT showing increases of approximately 1 mm as the shallow convection developed ahead of the system. This

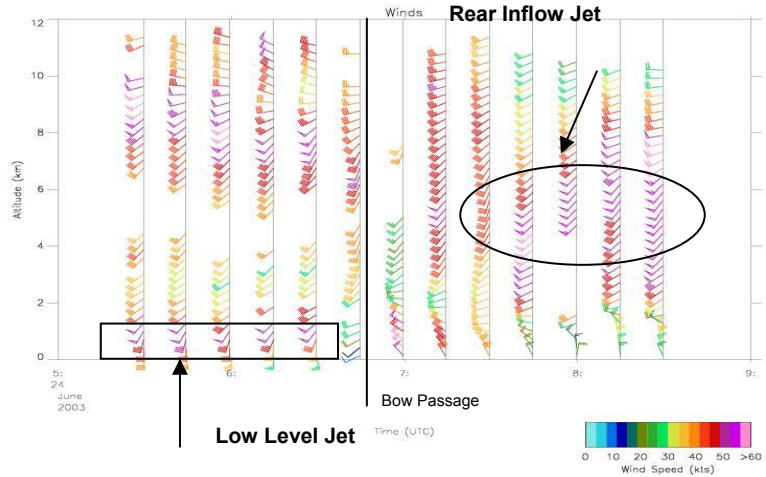


Figure 3: MIPS 915 MHz Profiler Winds

increase is an indication that the atmosphere was destabilizing, which in turn could support the shallow convection measured by the 915 MHz profiler.

3. STORM STRUCTURE

3.1 MIPS Observations

Fig. 2 presents a sequence of radar reflectivity images from the DMX WSR-88D for a 2-h period around the time of passage over the MIPS. The mesoscale organization of the MCS changed significantly over this period, from an orientation of west to east at 0446 UTC, to southwest to northeast by 0646 UTC. The initial bulge in the bow echo appeared around 0616 UTC and

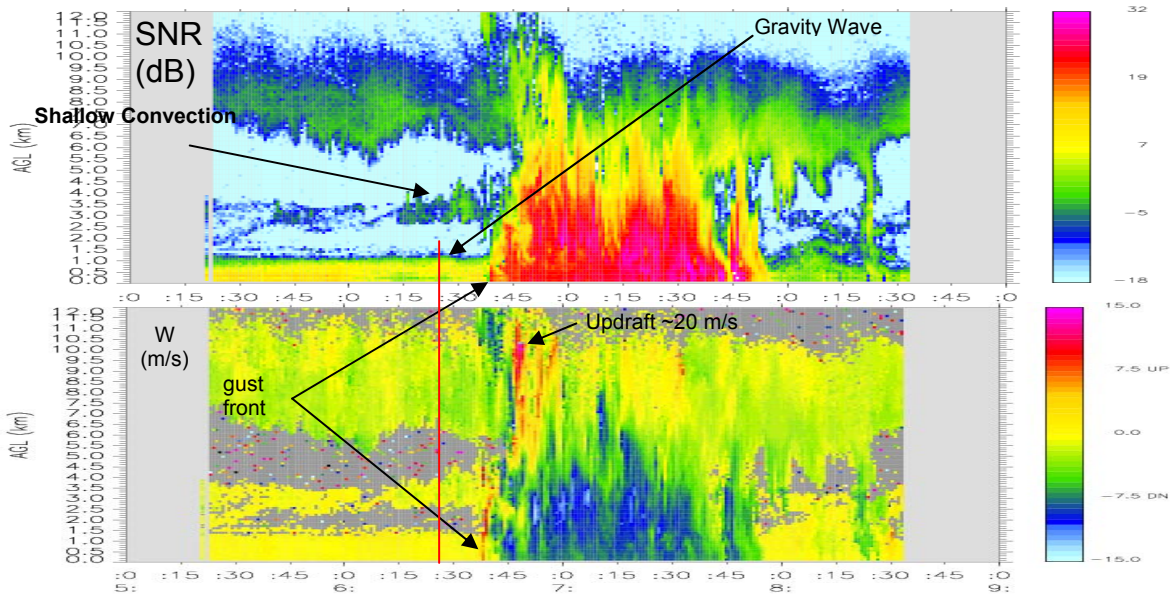


Figure 4: MIPS 915 MHz SNR and Vertical Velocity

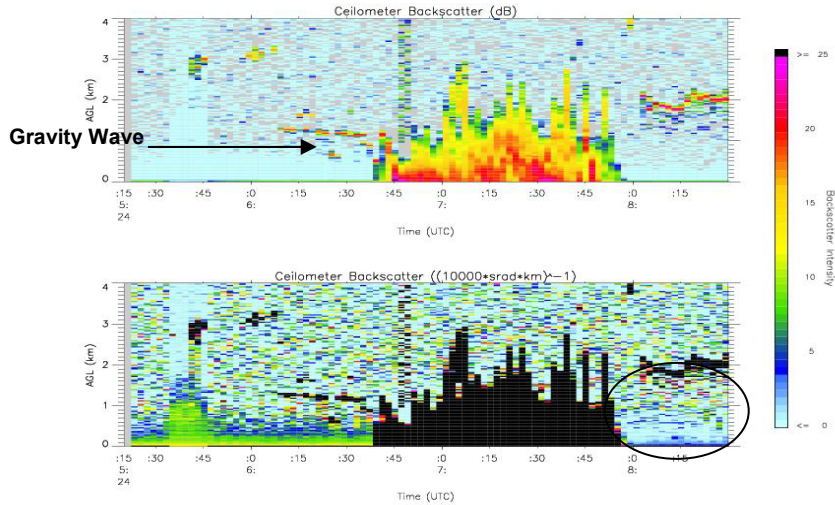


Figure 5: Time Height Series of MIPS Ceilometer. The top panel is ceilometer backscatter in units of dB. The bottom panel is backscatter in units of power. Heavy rain is denoted by the black color. The area in the circle shows how the atmosphere became more pristine after the passage of the bow.

became prominent by 0641 UTC, near the time of passage over the MIPS.

At 0621 the gust front emerged from the leading edge of precipitation, and accelerated ahead of the system. The gust front was sampled by the MIPS 17 min later at 0638, and is marked by a fine line in the SNR, and a narrow updraft in the W field in Fig. 4. The sequence of PPI images in Fig. 2 shows the passage of the bow echo apex directly over the MIPS, beginning near 0636 UTC. The origin of this outflow surge appears to be connected to the core of high Z , located west-northwest of the MIPS at 0526 and 0546 UTC. Thus, appreciable evolution in this segment of the bow echo occurred one hour prior to arrival over the MIPS.

The bow echo core between 0645 and 0710 UTC is depicted by large values of 915 SNR in Fig 4a, and high values of ceilometer backscatter in Fig. 5. A low-level updraft of about 10 m s^{-1} , confined to below 2.5 km, accompanied the sharp gust front sampled near 0638 UTC. A clear signature of the gust front passage is revealed in the surface measurements (Fig. 7), which reveals sharp wind shift and temperature drop. The

gust front updraft preceded the storm core updraft, shown as several maxima within the 4-12 km AGL altitude range. The maximum updraft is estimated at $\sim 20 \text{ m s}^{-1}$ near 10.5 km at 0645-0650 UTC. (Fig. 4). The maximum wind gust of 24 m s^{-1} occurred at approximately 0652 which corresponds with the distinct maxima in negative W near the 2.5 km level at 0652. Other distinct wind gusts at 0659 (16 m s^{-1}) and 0707 (13 m s^{-1}) were also recorded and correspond well with maxima in negative W at 0659 and 0707 UTC. If the terminal fall speed for rain is assumed (hail was not observed at the surface), downdrafts of $4\text{-}6 \text{ m s}^{-1}$ would result from the relation, $w = W - V_T$, in which

W is measured Doppler velocity (vertical incidence) and V_T is terminal fall speed.

The electric field mill (EFM) time series (Fig. 6) provides valuable information on storm properties based on measurements of the vertical component of the electric field, sampled at a rate high enough (50 Hz) to resolve lightning flashes. Local lightning flashes are represented as discontinuities (quasi-vertical lines) in the time series, and appear at frequent intervals, particularly within the bow echo core. Mesoscale features and subtle variations in the E field are apparent in several locations: a gravity wave passage at 0620, the gust frontal passage at 0638 UTC and electric field oscillations near the trailing portion, and within the wake, of the receding and weakening bow echo. These data will be analyzed in greater detail to relate the E field and lightning frequency to variations in the bow echo kinematic structure, determined from analysis of the Eldora radar data, summarized in the next section.

The microwave profiling radiometer (MPR) data, shown in Fig. 8, depict relative variations in

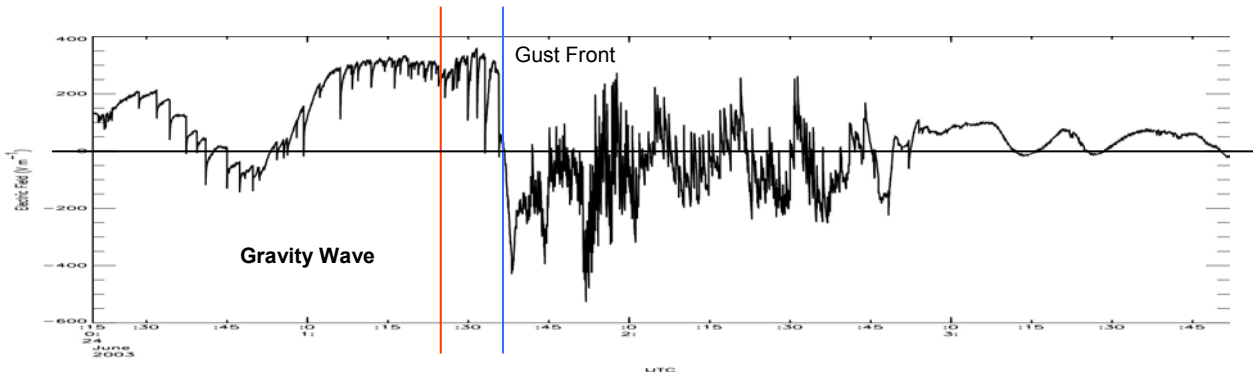


Figure 6: MIPS EFM Time Series. The gravity wave passage is denoted by the red line and gust front passage by the blue line. The neutral line is the black line across the time height series. Positive charge is above that line, and negative below it.

thermodynamic structure in non precipitating regions before and after storm passage. The MPR acquires soundings at high temporal resolution of 1 minute, but vertical resolution scales with height (i.e., greatest vertical resolution is near the surface). The MPR measured an increase in vertically integrated values of water vapor and cloud water prior to arrival of the bow echo, which is consistent with the 915 backscatter evolution also shown in fig. 4. Cooler and drier air was measured in the wake of the bow echo after 0715 UTC (when the radome water coating evaporated) which is shown by the lower values of relative humidity in the lower part of the atmosphere.

3.2 Eldora Observations

For the 24 June 2003 case the NRL-P3 and the NOAA P-3 both deployed in the same area as the ground crew. However the NOAA P-3 experienced an engine failure on route to the targeted area. For this case the radar data from the Eldora forward and aft tail radar will be analyzed. Figure 9 shows the track of the P-3 in reference to the MIPS location. For this case there are a total of three legs that are relevant to use for a comparison with MIPS measurements and for grasping

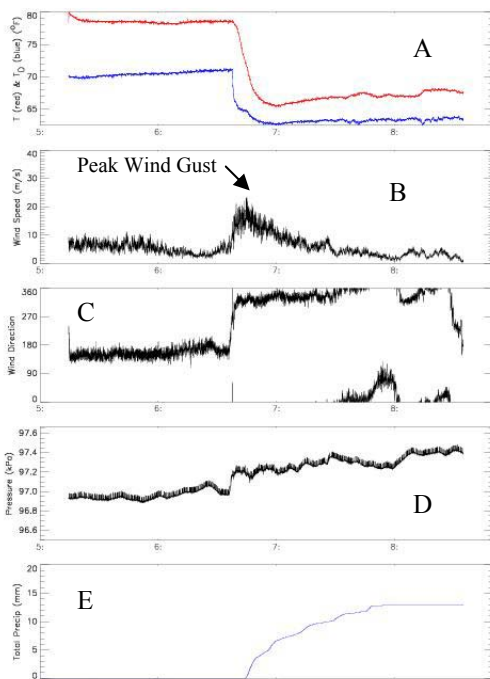


Figure 7: MIPS surface time series. a) Temperature is red, Dewpoint blue. b) Wind speed ($m s^{-1}$) c) Wind direction d) Pressure in kPa e) Total Precipitation

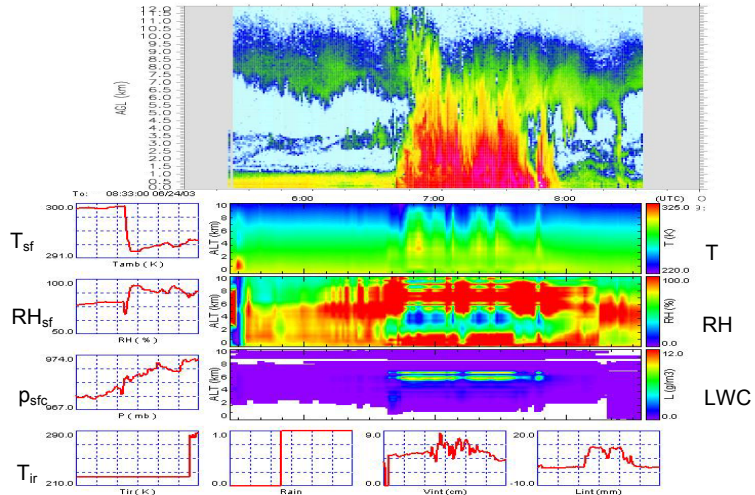


Figure 8: MIPS MPR Time Height Series. Temperature (top panel), relative humidity (middle panel), and liquid cloud water (bottom panel)

a better understanding of the structure of the bow echo system. Preliminary analysis of this data has shown radial velocities near $-40 m s^{-1}$ as the bow passed over the MIPS. Ground relative winds have shown the rear inflow jet, gust front, and outflow from the system. Figure 10 shows a scan from the Eldora fore radar as it passed near the MIPS during the bow echo passage. The top panel is reflectivity in units of dBZ and the bottom panel is the unfolded and corrected radial velocity data with the dual Doppler winds overlaid. This scan is a slice taken at $Z=1 km$ during leg2 which correlates to the time the bow passed over the MIPS. The surging portion is shown with velocities of $-30 m s^{-1}$ along the edge of the system, with higher values approaching $-40 m s^{-1}$. The reflectivity shows the apex of bowing segment as it passes over the MIPS. Recalling from earlier in the paper the 915 MHz Profiler showed a low level jet ($25 m s^{-1}$) that existed near 1 km AGL. This same rear inflow jet is shown in the reflectivity and velocity data. In the reflectivity it is the notch at the rear of the system, and in the velocity it is shown by the dual Doppler winds of approximately $30 m s^{-1}$ on the left side of the system.

4. GRAVITY WAVE

Approximately 10 minutes prior to the passage of the bow echo over the MIPS a fine line (produced by a gravity wave) was detected by the Des Moines WSR-88D radar (shown in the circular area of Fig. 2), MIPS ceilometer, and MIPS 915 MHz Doppler Profiler. The wave fine line is apparent in Fig. 11 between 0501-0626. This wave is resolved in 915 MHz vertical velocity data with a maximum updraft speed of about $1 m s^{-1}$. Shortly after this, the wave was not a visible feature in the DMX reflectivity field. Although this wave did not appear to have a direct influence on the MCS, gravity wave phenomena (including bores) may serve to

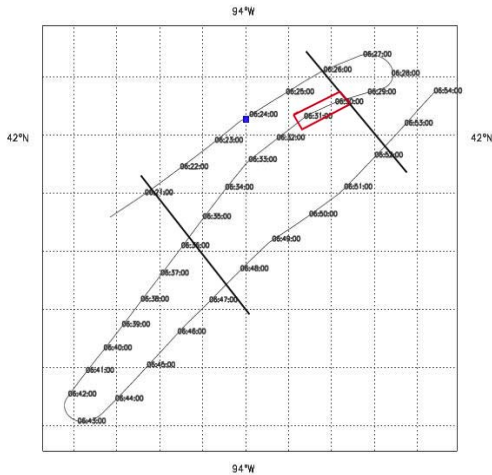
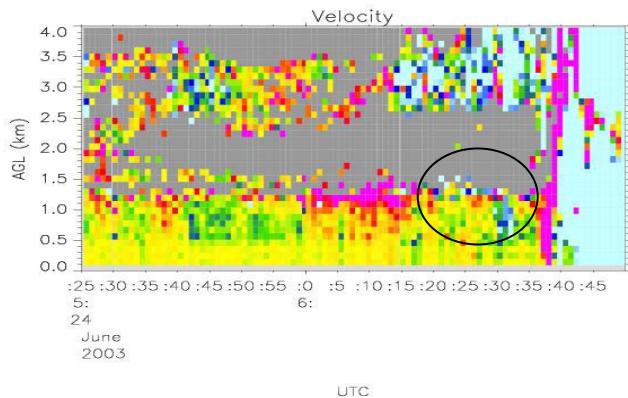


Figure 9: Flight Track of the Eldora (MIPS is located in the blue square) (Leg 1 is the top track, Leg 2 middle, and Leg 3 bottom track)

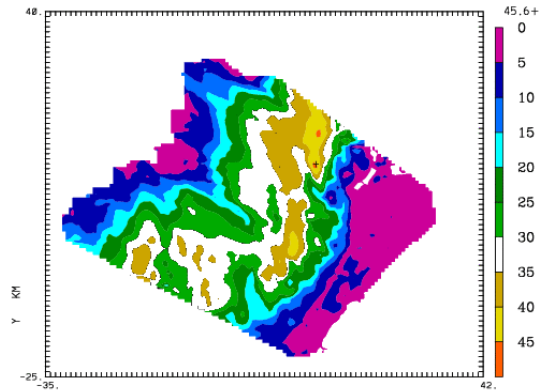
condition the pre-storm environment by destabilizing the atmosphere and lift water vapor to high levels.

5. CONCLUSIONS

The Bow echo system on 24 June 2003 that passed over the MIPS system had features not measured before. This system as it was passing over head was weakening, but it was surging with the greatest radial velocity (exceeding 30 m s⁻¹ from the DMX WSR-88D) as it passed over the MIPS. Several key features have been found in this analysis that include the pre-bow atmospheric state, internal storm structure, an interesting gravity wave that occurred before the bow passage, and post atmospheric structure. From this analysis it can be said that the environment ahead of a bow echo system must have high instability, which was the case here, cape values were in the 4000 J kg⁻¹ range. The upper level winds



**/06/24 06:31:02-06:36:02 COMBIN Z = 1.00 KM DBZF
(AS OF 08/27/04) ORIGIN=(0.00, 0.00) KM X-AXIS= 90.0 DEG



**/06/24 06:31:02-06:36:02 COMBIN Z = 1.00 KM VGF
(AS OF 08/27/04) ORIGIN=(0.00, 0.00) KM X-AXIS= 90.0 DEG

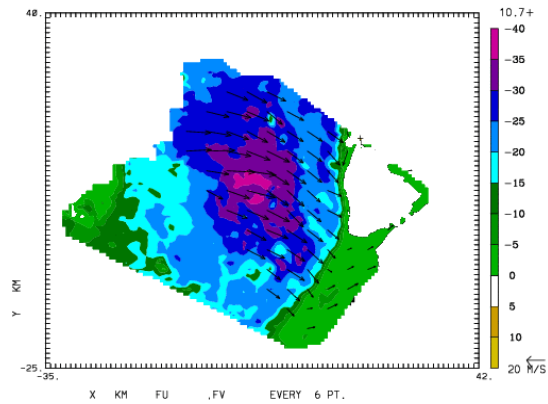


Figure 10: Eldora reflectivity for leg2 (Top) Eldora Radial Velocity for leg2 (Bottom). Rear Inflow jet is noticeable on the reflectivity (notched area), and in the velocity data.

must be westerly, there must be sufficient wind shear, and there needs to be a strong low level jet. Looking at the internal structure of the system it was found that the

bow echo is made up of several different cells, each having different structure and strength. It was interesting to note that in the stronger portions of the system the electric field was most likely positive, and stronger than the less intense portions of the bow echo. Post atmospheric conditions were much dry, and much more pristine than before the system passed over. This is shown by the MPR and the ceilometer data. This system was not a classic bow echo or the model bow echo because it lacked a large stratiform rain region behind it. However, most system that were studied during BAMEX did not fit into the model bow echo, so that leads to the question, is there a model bow echo? As future research advances hopefully this question can and will be answered. Future work in this area

involves integrating Eldora radar data with the MIPS and MClass Data. Distrometer data will also be used to further classify the internal storm structure, and drop size distribution.

7. REFERENCES

- Fujita, T. T., 1978: Manual of downburst identification for project NIMROD. Satellite and Mesometeorology Research Paper No. 156, Department of Geophysical Sciences, University of Chicago, 104 pp.
- Johns, R.H., 1982: A synoptic climatology of northwest flow severe weather outbreaks. Part 1: Nature and significance. *Mon. Wea. Rev.*, 110, 1653-1663.
- Johns, R.H., 1984: A synoptic climatology of northwest-flow severe weather outbreaks. Part 2: Meteorological parameters and synoptic patterns. *Mon. Wea. Rev.*, 112, 449-464.
- Johns, R.H., 1993: Meteorological conditions associated with bow echo development in convective storms. *Wea. and For.*, 8, 294-299.
- Johns, R.H. and W.D. Hirt, 1987: Derechos: Widespread convectively induced windstorms. *Weather and Forecasting*, 2, 32-49.
- Klimowski, B. A., R. Pyzybylinski, G. Schmocker, and M. R. Hjelmfelt, 2000: Observations of the formation and early evolution of bow echoes. Preprints, 20th Conf. on Severe Local Storms, Orlando, FL, Amer. Meteor. Soc., 44-47.
- Weisman, M. L., and J. B. Klemp, 1986: Characteristics of isolated convective storms. *Mesoscale Meteorology and Forecasting*, Amer. Meteor. Soc., Boston, 331-358.
- Weisman, M.L., J.B. Klemp, and R. Rotunno, 1988: Structure and evolution of numerically simulated squall lines. *J. Atmos. Sci.*, 45, 1990-2013.
- Weisman, M. L., 1992: The role of convectively generated rear-inflow jets in the evolution of long-lived mesoconvective systems. *J. Atmos. Sci.*, 49, 1826-1847.
- Weisman, M.L., 1993: The genesis of severe, long-lived bow-echoes. *J. Atmos. Sci.*, 50, 645-670.
- Weisman, M.L. and C. Davis, 1998: Mechanisms for the generation of mesoscale vortices within quasi-linear convective systems. *J. Atmos. Sci.*, 55, 2603-2622.